

Estimation COD_{Mn} in Guangzhou section of Pearl River based on GF-1 images

Y. B. Feng^{1,2}, Y. Q. He^{1,2}, Q. H. Fu^{1,2}, C. Q. Liu^{1,2}, H.Z. Pan^{1,2}, B. Yin^{1,2}

¹ Key Laboratory of dynamics and associated process of the Pearl River Estuary,
Ministry of water resources, China – (robinut, heyinqing@foxmail.com)

² Pearl River Hydraulic Research Institute, Guangzhou, China

KEY WORDS: COD_{Mn} , GF-1, water color remote sensing, Pearl River, Guangzhou

ABSTRACT:

Due to the way that remote sensing works, it has natural advantage to detect optical constituents in waters. And many kinds of inversion models were constructed based on the three main optical constituents, namely chlorophyll-a (Chl-a), suspended particulate matter (SPM), colored dissolved organic matter (CDOM). Except Chl-a used as an indicator of eutrophication, however, the public generally cares less about other two parameters and is more familiar with Grade I ~ V scheme for utilization and protection purposes. Notice the three main optical constituents are also organic-related to some extent. It offers a possible way to estimate COD_{Mn} via remote sensing. According to field measurement conducted along the Guangzhou section of Pearl River (GPR for short), the spatial variation of COD_{Mn} in GPR shows some kinds of geographical feature, so does the correlation between COD_{Mn} and water color constituents. It indicated the complicated contribution of COD_{Mn} in GPR or some other urban rivers. Based on the band setting of GF-1 satellite, two kinds of inversion model of COD_{Mn} in GPR were finally constructed. One directly achieved COD_{Mn} from regression models of which predictors were different band combinations in different channels of GPR. To make the study more practical, the other one first provided empirical models of the three optical constituents, and then estimated COD_{Mn} of GPR based on its relationship with optical constituents. After all, Chl-a, SPM and CDOM could be distinguished optically, and remote sensing models of these three constituents in other studies may also be available.

1. INTRODUCTION

1.1 General Instructions

In the field of water colour remote sensing, we centre on optical properties of water. Due to the longstanding civilization from mass media and elementary education, however, the public pays more attention to the water quality. The most striking distinction is that the Case 1 and Case 2 classification of waters is commonly used for bio-optical modelling while most citizens are familiar with Grade I ~ V scheme for utilization purposes and protection objectives. It leads to the three main optical constituents as chlorophyll-a (Chl-a), suspended particulate matter (SPM), colored dissolved organic matter (CDOM) retrieved by remote sensing are not aligned with pollution indicators such as chemical oxygen demand (COD), biochemical oxygen demand (BOD), total phosphorus (TP), ammonia nitrogen and heavy metals. This embarrassing mismatch restricts the application of remote sensing in the field of water monitoring.

Take permanganate index (COD_{Mn}) as an example, it is one of important parameters used to assess organic pollution in surface water and ground water (Tian et al., 2008). Before remote sensing comes into view, field sampling and indoor testing form the primary method and provide us the credible COD_{Mn} values (Baker et al., 1999; Udovichenko and Nabivanets, 2001; Udovichenko et al., 2001). But it is a time-consuming and laborious work, and is impossible to acquire real-time and large-scale data for monitoring. That's instead the advantage where remote sensing lives by. So remote sensing has been applied more and more widely in the water quality monitoring recently.

For instances, Fu et al (2007) took the Grand Canal through southern Jiangsu as the studied area and found Band 1 of Landsat TM images was highly correlated with COD_{Mn} ; Wang et al (2003) constructed a BP neural network model to inverse COD_{Mn} of Poyang Lake from TM data; Yang et al (2007) employed TM images of Tai Lake to retrieve COD_{Mn} based on the empirical relationship with Chl-a which is computed by a semi-empirical method; still the Tai Lake, Tao et al (2014) proposed an Advanced COD_{Mn} Forecast Index (ACFI) to estimate COD_{Mn} using Landsat-8; Hao et al [2011a, 2011b] found the ratio of TM3 and TM5 had high relevance with COD_{Mn} of Daliangdian Reservoir; Wang et al (2011) applied a support vector regression (SVR) method to predict COD_{Mn} in the Weihe River by SPOT-5 data.

Obviously, there are not unified methods to estimate COD_{Mn} of inland waters. Despite the different band response of satellite sensors, the most important reason is that the COD_{Mn} is a synthetical index rather than a certain substance like Chl-a. It refers to the amount of oxygen consumed when the organic matter in a given volume of water is chemically oxidized to CO_2 and H_2O by permanganate (Xia, 2005). And this organic matter is constructed with organic particulate matter and dissolved organic matter in any proportions. Considering the various spectral characteristics of organics in different aquatic environments, it's necessary to re-establish the inversion method of COD_{Mn} in regional studies.

The Pearl River is an extensive river system in southern China and supplies water to numerous cities. Among them, the Guangzhou City which serves as a political-economic-cultural centre of Guangdong province is the most populous one. So pollutants like industrial waste, sewage runoff and agriculture discharges all make the water quality of this section declined. Nevertheless, only few studies have been published on the

application of remote sensing in contamination assessment of the Guangzhou section of the Pearl River (GPR for short). Wang et al (2001) recognized water pollution from TM images by qualitatively analysing the gray scale variation of each band due to organic pollutants. The result was practical because it visually displayed different levels of water quality in line with GB3838-88 where the Grade I~V scheme of surface water is proposed. Fan and Chen (2009, 2012) computed comprehensive pollution index of water quality based on referenced values of the Grade III water, and then established regression models of this index and TM bands to present water pollution. It's a quantitative attempt about this area, but the robust of the multiple linear regression and the practice that a single grade was referenced are worth discussing.

Therefore, this study is an extension of the previous effort, targeting on quantitatively estimating COD_{Mn} of the GPR and emphasizing on the regional relationship between COD_{Mn} and water colour constituents in order to combine well-developed water colour models. After all, Chl-a, SPM and CDOM could be distinguished optically. A remote sensing model for the retrieval of these three constituents may achieve more credible result. To make the study more practical, we also provide an empirical method to get COD_{Mn} directly from remote sensing images, like GF-1.

2. DATA ACQUISITION

In strict sense, GPR ranges from the mountain areas in the north (Baiyun Mountain) to sea level at the confluence of Pearl River in the south.

On 5~6 August 2015, field measurement was conducted along the Guangzhou section of Pearl River. As shown in Figure 1, there were 27 sampling sites where water samples were collected for Chl-a, SPM, CDOM and COD_{Mn} test in laboratory; bottom sediments were collected for water-tank experiment; and water surface spectral were recorded in situ according to above-water method (Tang et al., 2004).

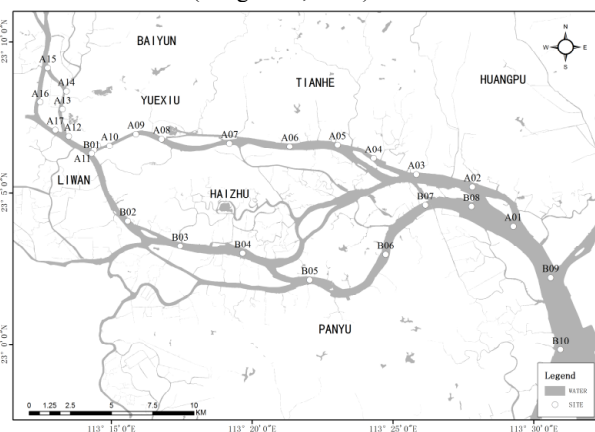


Figure 1. Sampling sites distribution of GPR

3. RESULTS AND DISCUSSIONS

3.1 Spatial variations of COD_{Mn} in GPR

From the field measurement, the lowest COD_{Mn} (2.8 mg/L) appeared at B3 and B4 located along the back-channel (Hou Hangdao) of GPR while the highest (7.2 mg/L) was found at A11, A14 and A15 all in the west-channel (Xi Hangdao). It

indicated that the degree of organic contamination of GPR may have some kinds of regional feature. Thus all the sampling points were divided into 3 groups geographically: a) the west channel represented by A11~A17; b) the front-channel represented by A01~A10; c) the back-channel represented by B01~B10.

As shown in the boxplot (Figure 3), the median values of COD_{Mn} decreased from west-channel, front-channel to back-channel, so do the data ranges and other statistical values. The maximum COD_{Mn} of front-channel denoted by the upper edge was found at A06 which was around LieDe, the downtown area of Guangzhou. For the outlier of back-channel, which was greater than the threshold exceptions $q3 + w \times (q3 - q1)$ in a boxplot ($q1$, the lower quartile; $q3$, the upper quartile; w , the 1.5 standard deviations), it's recorded in B01 where was just the downstream of west-channel. These spatial features of COD_{Mn} were basically in line with previous studies (Wang et al., 2001; Ma et al., 2003; Wang et al., 2009). So we regrouped sampling sites and the B01 was moved to the west-channel for subsequent analysis.

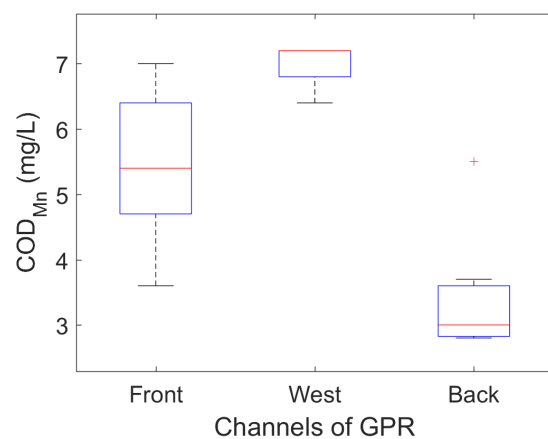


Figure 2. Comparison of COD_{Mn} in different parts of GPR

3.2 Relationships between COD_{Mn} and optical constituents

As a synthetic index of water pollutions, COD_{Mn} indicates the organic content in water. The three kinds of water colour constituents which remote sensing concerned are also organic-related to some extent. Generally speaking, Chl-a is considered to be the proxy for phytoplankton; SPM is divided into organic and inorganic components; CDOM as the abbreviation of colored dissolved organic matter is definitely organic. So the correlation coefficients between COD_{Mn} and water colour constituents were computed based on the regional division in section 3.1, and the result was shown in Table 1.

R	Chl-a	SPM	ag440
Front-channel	0.613	0.436	0.546
Back-channel	0.820	0.068	0.550
West-channel	-0.063	0.717	0.933
All field sites	0.860	0.520	0.743

Table 1. Correlation coefficients between COD_{Mn} and water colour constituents in GPR

3.2.1 West-channel: For the west-channel, COD_{Mn} was closely tied to ag_{440} , the absorption coefficient of CDOM at 440 nm normally as its concentration, and the correlation coefficient R was up to 0.933. The correlation between COD_{Mn} and SPM was also relatively high ($R = 0.717$), however, the concentration variation of SPM under a high concentration of COD_{Mn} (about 7.2 mg/L) was quite large compared with those of CDOM (Figure 3). As for Chl-a, the correlation was negligible. Therefore, the COD_{Mn} in the west-channel of GPR could be estimated from ag_{440} and their relationship is constructed as Eq-1

$$y = 8.108x^{0.4243}, R^2 = 0.8512 \quad (1)$$

where $y = COD_{Mn}$
 $x = ag_{440}$

At this point, different regression models were tried to quantify this relationship. From the numerical perspective, a complicated regression function may generate high value to evaluate fitting precision (e.g. R^2), but the possibility of sudden changes outside the range of training data (over-fitting) could make this model far away from the actual. So only linear polynomial, one-term exponential model and one-term power model were considered based on the sampling data. As shown in Figure 4, all the three regression functions reflect the COD_{Mn} variation with ag_{440} quite well and achieve high R^2 . However, only the power function gives a reasonable trend when the COD_{Mn} concentration is below 5 mg/L.

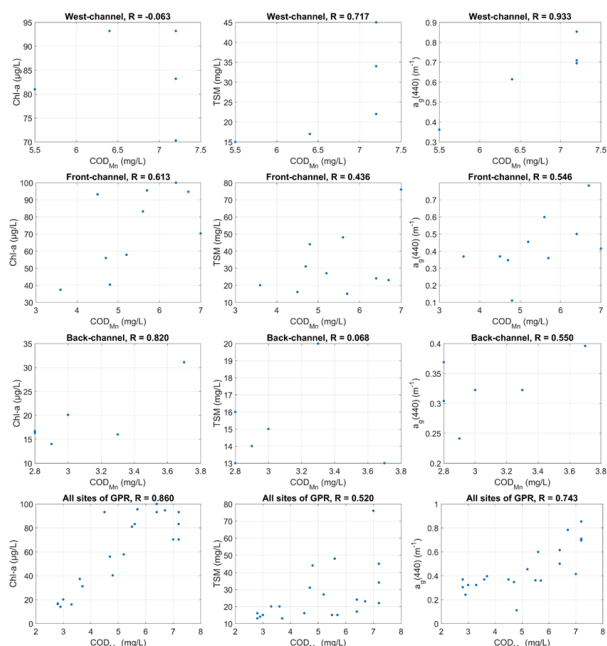


Figure 3. Measured values of water colour constituents versus COD_{Mn} in different parts of GPR

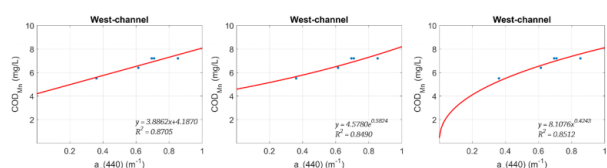


Figure 4. Different fitting curves of COD_{Mn} and ag_{440} in west-channel of GPR

3.2.2 Front-channel: For the front-channel, the correlation coefficients between COD_{Mn} and three optical constituents are all around 0.5, an embarrassing value. It says that 1) the COD_{Mn} of this channel could hardly be obtained from either one of optical constituents; 2) the hydrodynamic condition (or water environment) here is more complicated so that some measurements are unsuited to analysis together; 3) the main contribution to COD_{Mn} here is non-optical ingredients. The latter possibility stands outside the discussion owing to the required data is beyond the scope of this paper.

For the first possibility, multivariate linear regression was used to evaluate the combined contribution of optical constituents to COD_{Mn} . We found that the R^2 statistic decrease from 0.768 to 0.428, and the predictor variables were respectively all-the-three-optical-constituents and Chl-a- ag_{440} . So the COD_{Mn} of this channel may be predicted by Eq-2.

$$y = 5.7687 + 1.6545x_1 + 1.7073x_2 + 0.7260x_3, R^2 = 0.7682 \quad (2)$$

where $y = COD_{Mn}$
 $x_1 = Chl-a_N$
 $x_2 = SPM_N$
 $x_3 = ag_{440_N}$

The subscript N indicated that the predictors were all scaled between -1 and 1 by normalizing the minimum and maximum values of each optical constituent. The minimum values were all set to 0, and the maximum values were respectively 120 $\mu\text{g/L}$ of Chl-a, 80 mg/L of SPM and 0.8 m^{-1} of ag_{440} on a comprehensive basis of several studies in GPR (Fan, 2012; Wang et al., 2009; Ma et al., 2003; Li et al., 2013; Jiang et al., 2010).

For the second possibility, the scatter plots of COD_{Mn} v.s. each optical constituent are displayed in Figure 3. It's observed that 1) the correlation between COD_{Mn} and Chl-a would become significant ($R = 0.903$) if sample points A3 and A5 were removed, whose Chl-a concentrations were respectively 93.2 $\mu\text{g/L}$ and 70.3 $\mu\text{g/L}$; 2) the correlation coefficient between COD_{Mn} and SPM would be raised to 0.894 if sample points A8~A10 were removed, which SPM concentration were 15 mg/L, 24 mg/L, 23 mg/L successively; 3) the correlation coefficient between COD_{Mn} and ag_{440} would increase to 0.752 if A1 and A5 were not considered, which ag_{440} were 0.368 m^{-1} and 0.415 m^{-1} respectively. Upon these assumptions, we located the points removed and found they were all near docks or factories (Table 2). However, it's hard to identify whether the discharge of industrial wastewater was normal condition because the removal of deferent sites would generate different sensitive parameter to COD_{Mn} . In consequence, the analysis of this possibility didn't bring about any quantitative results.

Sampling sites	Nearby buildings
A01	Nanghai shipyard
A03	Yuzhu shipyard, Jiali wharf
A05	Yongxing tile factory, Guangzhou Paian Concrete Ltd
A08	Sha Tau cruise terminal
A09	Tianzi Wharf
A10	Xidi Wharf

Table 2. Abnormal sites of the front-channel and the buildings around

3.2.3 Back-channel: For the back-channel, Chl-a became the highly referential constituent of COD_{Mn} since their correlation coefficient was 0.820, way above other parameters. As in the west case, the COD_{Mn} here could be simply modelled in Eq-3.

$$y = 1.2333x^{0.3137}, R^2 = 0.6432 \quad (3)$$

where $y = \text{COD}_{Mn}$
 $x = \text{Chl-a}$

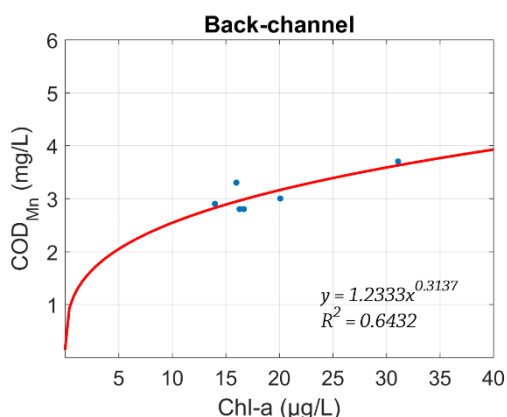


Figure 5. The fitting curve of COD_{Mn} and Chl-a in back-channel of GPR

3.2.4 All sites of GPR: Given all the sites of GPR, each optical constituent behaved certain correlation against COD_{Mn}, and the links decreased as follow: Chl-a, ag440, TSM (Figure 4). Despite different grades, all the scatter trends shared the same feature that the correlation became impaired as COD_{Mn} increased. As a result, even if Eq-4 employed Chl-a to acquire COD_{Mn} concentration of GPR and it worked out fine (R² = 0.767), Eq-1 was still recommended to evaluate high COD_{Mn} (i.e. those above 6 mg/L for GPR) which was more likely to be found in west-channel. This further indicated the complicated contribution of COD_{Mn} in GPR or some other urban rivers.

$$y = 0.8832x^{0.4367}, R^2 = 0.7666 \quad (4)$$

where $y = \text{COD}_{Mn}$
 $x = \text{Chl-a}$

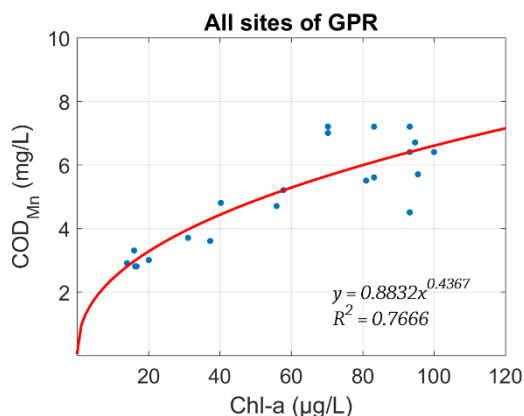


Figure 6. The fitting curve of COD_{Mn} and Chl-a in back-channel of GPR

3.3 Remote sensing retrieval of COD_{Mn}

Benefiting from high spatial resolution and low revisit period, the GF-1 satellite is now widely used in many domestic industries. The PMS optical sensor on-board could acquire 2m resolution images in visible and near-infrared bands (Blue, 450-520nm; Green, 520-590nm; Red, 630-690nm; NIR, 770-890nm), and offer a new way to monitor water qualities in urban.

On basis of regional features of GPR COD_{Mn} discussed above, two kinds of inversion models were constructed. One of them directly achieved COD_{Mn} from regression models of which predictors were different band combinations in different channels of GPR. The combinations include common forms such as x_1 , x_1/x_2 , $x_1/(x_1+x_2)$, $(x_1-x_2)/(x_1+x_2)$, $x_1/(x_1+x_2+x_3)$, $(x_1 \pm x_2)/(x_1+x_2+x_3)$, etc. And each form was constructed by different bands. After comparing the fitting performance, regression equations with the highest R² was shown in Figure 8. For the front and west channels, the R² were both above 0.65 and the fitting results were acceptable. For the back-channel, the statistic R² was just 0.27 although the fitting curves made a roughly good prediction. In order to make up for the lack of measurements, all sites of GPR were assembled and the band combination B3/(B1+B4) was selected to get COD_{Mn} not only in the whole GPR but also the back-channel.

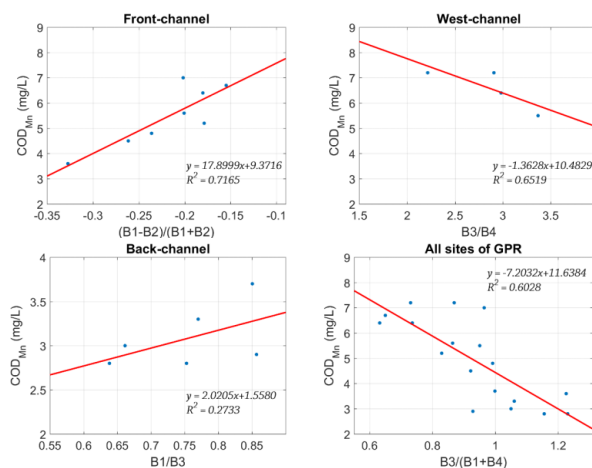


Figure 7. The COD_{Mn} regression models based on GF-1 PMS band setting

To make our study more practical, the other one first provided empirical models of the three optical constituents, and then estimated COD_{Mn} of GPR based on its relationship with optical constituents discussed above. After all, Chl-a, SPM and CDOM could be distinguished optically, and remote sensing models for the retrieval of these three constituents in other studies may also be available. According to measurement, the fitting equation of Chl-a, SPM and ag440 of each channel was constructed and shown in Table 3~5.

	x	Fitting equation	R ²
Front	B3/(B2+B4)	$y = -236.15x + 219.91$	0.700
Back	B2	$y = 0.001x^{-2.618}$	0.554
West	B1/(B3+B4)	$y = 40.358 \exp(1.092x)$	0.679
GPR	(B1+B3)/(B1+B2+B4)	$y = 11.322x^{-5.653}$	0.686

Table 3. The Chl-a regression models of GPR channels based on GF-1 PMS band setting

	x	Fitting equation	R^2
Front	$(B1+B3)/(B1+B2+B3)$	$y=3.174*10^{-10} \exp(42.808x)$	0.810
Back	$(B1+B3)/(B1+B2+B4)$	$y=0.264\exp(4.965x)$	0.835
West	$(B2+B4)/(B1+B2+B3)$	$y=9.892*10^{22}x^{-79.84}$	0.792
GPR	$B2/(B3+B4)$	$y=25.094x^{-2.149}$	0.224

Table 4. The SPM regression models of GPR channels based on GF-1 PMS band setting

	x	Fitting equation	R^2
Front	$B1/B3$	$y=0.09\exp(1.89x)$	0.500
Back	$(B1+B4)/(B1+B2+B3)$	$y=-1.25x+0.727$	0.402
West	$(B2+B3)/(B1+B2+B3+B4)$	$y=4.198x+3.375$	0.587
GPR	$(B2+B4)/(B1+B2+B3)$	$y=2.949x-1.059$	0.383

Table 5. The ag440 regression models of GPR channels based on GF-1 PMS band setting

It's found that 1) the fitting R^2 of ag440 was generally low, so the first kind of COD_{Mn} inversion model (the direct one) may be more suitable to achieve COD_{Mn} in west and front channels; 2) the fitting R^2 of SPM in the three channels were all above 0.79 while this value fell to 0.22 considering all sites of GPR, it indicated the dominant component of SPM in each channel may be different.

Upon these fitting equations, four GF-1 PMS images (imaging date: Dec. 7, 2016) of GPR were employed to get the COD_{Mn} distribution. As displayed in Figure 8, the spatial trend of inversion result basically coincided with field measurements. The COD_{Mn} of back-channel were lower than those of other two parts of GPR in general. And it showed that the COD_{Mn} values of GPR ranged mainly between 4 mg/L to 8 mg/L, roughly belonging to Grade III~IV waters according to Environmental Quality Standards for Surface Water (GB 3838-2002).

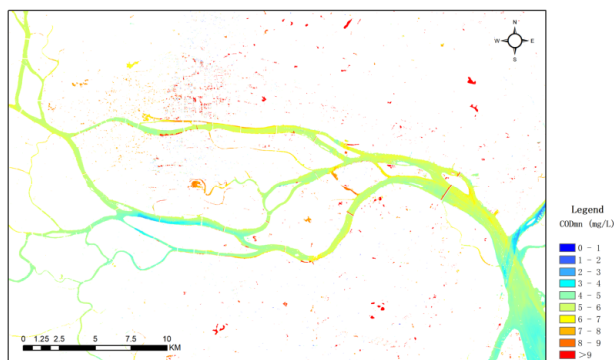


Figure 8. The inversion result of COD_{Mn} in GPR based on GF-1 PMS images

4. CONCLUSION

Based on field measurement of GPR, this study divided the urban river into three channels and analysed the correlation between COD_{Mn} and the three water colour constituents (Chl-a, SPM and CDOM) in the remote sensing domain, then constructed two kinds of COD_{Mn} inversion models suitable for GF-1 images.

These analysis indicated that: 1) the COD_{Mn} concentration of west-channel was lower than other part of GPR in general; 2) the COD_{Mn} of west-channel and back-channel was respectively dominated by CDOM and Chl-a while that of front-channel was contributed by all the three optical constituents; 3) the

COD_{Mn} showed higher correlation with Chl-a on the whole of GPR; 4) the COD_{Mn} inversion directly from band combinations of GPF-1 images was applied here, but the acquisition of COD_{Mn} from optical constituents also recommended because it provided an open port and could be referenced from other studies; 5) the inversion COD_{Mn} based on GF-1 images (Dec. 7, 2016) showed the water quality of GPR mainly belonged to Grade III~IV.

In view of the complicated contribution of COD_{Mn} in GPR, this study hold the point that water qualities retrievals via remotely sensed images should take regional characteristics and composition of target parameter into consideration.

ACKNOWLEDGEMENTS

Acknowledgements of support for the projects: Estimation and Forecast of Suspended Sediment Concentration in the Pearl River Estuary from Remote Sensing Images based on Data Assimilation Algorithm (Natural Science Foundation of Guangdong, China, NO. 2017A030313232)

Remote Sensing Identification and Dynamic Monitoring of Urban Black-Odor Water Bodies based on Chroma Parameters: A Case Study in Guangzhou (Science and Technology Program of Guangzhou, China, NO. 201804010270).

REFERENCES

- Baker, J. R., Milke, M. W., & Mihelcic, J. R., 1999. Relationship between chemical and theoretical oxygen demand for specific classes of organic chemicals. *Water Research*, 33(2), pp. 327–334.
- Fan, F., 2012. Monitoring and Analyzing Water Pollution of the Pearl River in Guangzhou Section by Using Remote Sensing Images and Field Acquisition Data. *Advances in Information Sciences & Service Sciences*, 4(8), pp. 67–75.
- Fan, F. L., & Chen, B., 2009. Spatial Analysis of Water Quality of Pearl River Guangzhou by Reach Using TM Data Under the Supporting of GIS. *Environment & Ecology in the Three Gorges*, 2(1), pp. 12–16.
- Fu, J., 1993. Correlative Analysis between the Reflection Spectrum and Pollution Coefficients of Water in the Grand Canal through Southern Jiangsu. *Environmental Science*, 14(5), pp. 13–18.
- Hao, H. S., 2011. Multi-spectral RS Inversion of COD_{Mn} in Micro-polluted Water. *Journal of Anhui Agricultural Sciences*, 39(12), pp. 7363-7364.
- Hao, H. S., Cao, Z. Y., Jin-Ping, M. O., & Liang-Qing, W. U., 2011. A Quantitative Study of COD_{Mn} in Land Reservoirs in High-fluoride Areas. *China Rural Water & Hydropower*, (6), pp. 44-48.
- Jiang, Q., Hou, W., Gu, J., Peng, L., & Lei, L., 2010. Nutritional status and population characteristics of Cyanobacteria in small and medium sized reservoirs in Guangzhou, southern China. *Ecology and Environmental Sciences*, 19(10), pp. 2461–2467.
- Li, P., Gui, C., & Guan, X., 2013. Investigation on the Eutrophication Status of the Pearl River Guangzhou Section

- during Drought Period. *Journal of Anhui Agri. Sci*, 41(11), pp. 4961 – 4963.
- Ma, Y., Wang, Y., & Jia, G., 2003. Application of Remote Sensing in Monitoring Water Pollution in Guangzhou Section of the Pearl River. *Chongqing Environmental Science*, 25(3), pp. 13–16.
- Tang, J., Tian, G., Wang, X., Wang, X., & Song, Q., 2004. The Methods of Water Spectra Measurement and Analysis I :Above-Water Method. *Journal of Remote Sensing*, 8(1), pp. 37 – 44.
- Tao, Y., Xu, M., & Ma, J., 2014. Estimation of COD_{Mn} in Tai lake basin using Landsat-8 satellite. In *Geoscience and Remote Sensing Symposium*, pp. 3866–3869.
- Tian, J., Yonggang, H. U., & Jie, Z., 2008. Chemiluminescence detection of permanganate index (COD_{Mn}) by a luminol-KMnO₄ based reaction. *Journal of Environmental Sciences*, 20(2), pp. 252–256.
- Udovichenko, V. V., & Nabivanets, B. I., 2001. Methods for Determination of Chemical Oxygen Demand in the Natural Waters. *Hydrobiological Journal*, 37(5), pp. 18.
- Udovichenko, V. V., Nabivanets, V. I., & Sukhin, V. V., 2001. Accelerated Method for the Determination of Chemical Oxygen Demand in the Natural Waters. *Hydrobiological Journal*, 37(2), pp. 8.
- Wang, J., Cheng, S., Jia, H., Wang, Z., & Tang, U. W., 2003. An artificial neural network model for lake color inversion using TM imagery. *Chinese Journal of Environmental Science*, 24(2), pp. 73.
- Wang, X., Fu, L., & He, C., 2011. Applying support vector regression to water quality modelling by remote sensing data. *International Journal of Remote Sensing*, 32(23), pp. 8615–8627.
- Wang, Z., Hu, R., Gu, Y., Song, S., Zhu, D., & Huang, Z., 2009. Community structures of periphytic algae in the Guangzhou reaches of the Pearl River and their relationship to water quality. *Acta Scientiae Circumstantiae*, 29(7), pp. 1510–1516.
- Wang, Zhaohui, Ren, H. U., Yangguang, G. U., Song, S., & Zhu, D., 2009. Community structures of periphytic algae in the Guangzhou reaches of the Pearl River and their relationship to water quality. *Acta Scientiae Circumstantiae*, 29(7), pp. 1510–1516.
- Xia, X. H., 2005. Influence of Humic Substance in Solids on the Measurement of Oxygen-Consuming Organics of the Yellow River. *Journal of Environmental Informatics*, 6(1), pp. 51–57.
- Yang, Y. P., Wang, Q., & Xiao, Q., 2007. Eutrophication Evaluation of Taihu Lake Based on Quantitative Remote Sensing Inversion. *Geography and Geo-Information Science*, 23(3), pp. 33–37.
- Yang, Y. P., Wang, Q., Xiao, Q., & Wen, J. G., 2006. Quantitative Remote Sensing Inversion Methods of Chlorophyll-a Concentration in Taihu Lake Based on TM Data. *Geography and Geo-Information Science*, 22(2), pp. 5–8.
- Yunpeng, W., Yushun, M. I. N., Jiamo, F. U., & Guoying, S., 2001. Remote Sensing Method of Water Pollution and Application on Water Pollution Monitoring in Guangzhou Section of Pearl River. *Journal of Remote Sensing*, 5(6), pp. 460–465.